FIGURE S1

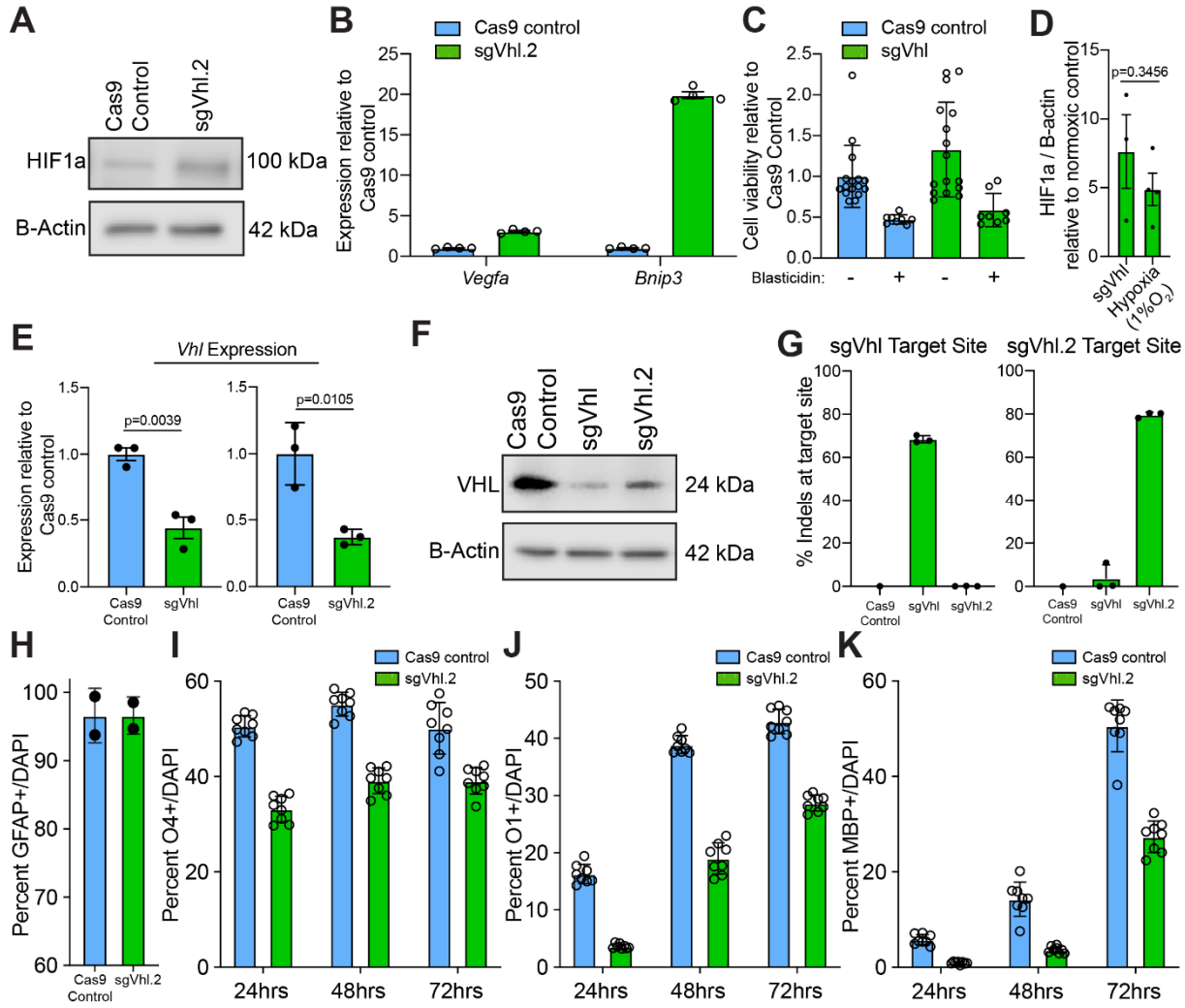

Figure S1. HIF1a Accumulation Impairs the Induction of Oligodendrocytes from OPCs, Related to Figure 1.

(A) Western blot of HIF1a of sgVhl.2 OPCs compared to Cas9 control OPCs. Data represent results from a single biological replicate.
(B) qRT-PCR of *Vegfa* and *Bnip3* in sgVhl.2 OPCs (in green) compared to Cas9 control OPCs (in blue). Data are presented as mean ± SEM from 4 technical replicates (individual wells).
(C) MTS assay of sgVhl OPCs compared to Cas9 control OPCs normalized to Cas9 control OPCs using a lethal dose of blasticidin (10μg/mL) as a positive control for cell death. Data are represented as mean ± SD from 8-16 technical replicates (individual wells).
(D) Quantification of the ratio of HIF1a to B-actin in sgVhl OPCs and physiological hypoxia (1% O_2) relative to respective normoxic controls. Data are presented as mean ± SEM from 3-4 biological replicates. p-value was calculated using Student's two-tailed t-test.
(E) qRT-PCR of *Vhl* in both sgVhl and sgVhl.2 OPCs (both in green) compared to Cas9 control OPCs (in blue). Data are presented as mean ± SEM from 3 independent biological replicates. p-values were calculated using Student's two-tailed t-test.

(F) Western blot of VHL of sgVhl and sgVhl.2 OPCs compared to Cas9 control OPCs.
(G) In-del analysis utilizing Outknocker software on PCR products surrounding sgRNA cut sites for both sgVhl and sgVhl.2 OPCs compared to Cas9 control. Data are presented as mean ± SD from 3 biological replicates.
(H) Quantification of the percentage of astrocytes (GFAP+ cells/ DAPI) formed from sgVhl.2 OPCs (in green) compared to Cas9 control OPCs (in blue). Data are presented as mean ± SD from 2 biological replicates.
(I-K) Quantification of the percentage of early O4+ (G), intermediate O1+ (H), and late MBP+ (I) oligodendrocytes formed from sgVhl.2 OPCs (in green) compared to Cas9 control OPCs (in blue) at day 1, 2 and 3 of differentiation. Data are presented as mean ± SD from 8 technical replicates (individual wells).

FIGURE S2

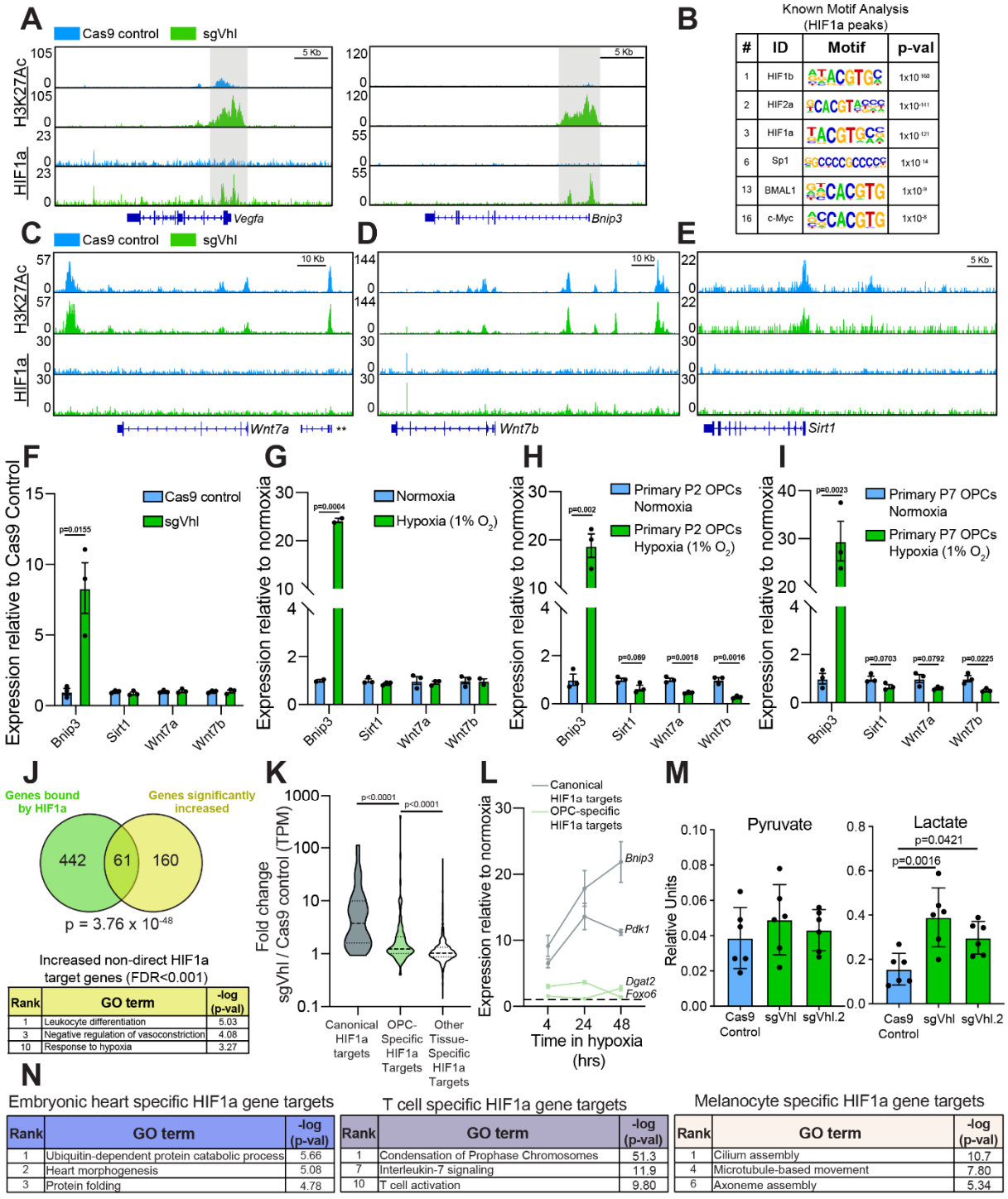

#	ID	Motif	p-val
1	HIF1b		1x10-160
2	HIF2a		1x10-141
3	HIF1a		1x10-121
6	Sp1		1x10-14
13	BMAL1		1x10-9
16	c-Myc		1x10-8

Rank	GO term	-log (p-val)
1	Leukocyte differentiation	5.03
3	Negative regulation of vasoconstriction	4.08
10	Response to hypoxia	3.27

Rank	GO term	-log (p-val)
1	Ubiquitin-dependent protein catabolic process	5.66
2	Heart morphogenesis	5.08
3	Protein folding	4.78

Rank	GO term	-log (p-val)
1	Condensation of Prophase Chromosomes	51.3
7	Interleukin-7 signaling	11.9
10	T cell activation	9.80

Rank	GO term	-log (p-val)
1	Cilium assembly	10.7
4	Microtubule-based movement	7.80
6	Axoneme assembly	5.34

Figure S2. HIF1a directly upregulates unique targets in OPCs, Related to Figure 2.

(A) Genome browser view of HIF1a signals in Cas9 control (in blue) and sgVhl (in green) OPCs at the locus for *Vegfa* and *Bnip3*. HIF1a accumulation in sgVhl OPCs is highlighted in gray. Scale bars, 5Kb.

(B) Table of known motifs significantly enriched under HIF1a peaks in sgVhl OPCs (FDR<0.001) displaying the transcription factor name, motif, and p-value ranked in order

of significance (# indicates rank out of all motifs from the analysis). See also Table S3 for full list of ranked motifs.
(C-E) Genome browser view of HIF1a and H3K27Ac ChIP-seq in Cas9 control (in blue) and sgVhl (in green) OPCs at the locus for *Wnt7a* (C), *Wnt7b* (D), and *Sirt1* (E). Scale bars, 10Kb, 10Kb, and 5Kb respectively. ** is 4930471M09Rik.
(F-I) qRT-PCR of *Bnip3*, *Sirt1, Wnt7a* or *Wnt7b* in Cas9 control OPCs (in blue) and sgVhl OPCs (in green) (F), OPCs treated with normoxia (in blue) or hypoxia (1% O_2, in green) (G), primary postnatal day 2 (P2) *in vivo* derived mouse OPCs cultured in physiological hypoxia (1% O_2, in green) compared to normoxia (in blue) (H), and primary immunopanned postnatal day 7 (P7) *in vivo* derived mouse OPCs cultured in physiological hypoxia (1% O_2, in green) compared to normoxia (in blue) (I). Data are presented as mean ± SEM from 3 independent biological replicates. p-values were calculated using Student's two-tailed t-test.
(J) Venn diagram showing the significant overlap (hypergeometric p-value= $3.76x10^{-48}$) of genes that are both direct targets of HIF1a (FDR<0.001) and significantly increase in sgVhl OPCs compared to Cas9 only control OPCs (p-adj <0.05). GO analysis was performed on genes that significantly increase but were not called as high stringency HIF1a peaks. The chart includes curated pathways with their rank based on their respective p-values.
(K) Violin plot of fold change in expression (TPM) between Cas9 control and sgVhl OPCs of genes included in canonical (dark gray), OPC-specific (light green) and " other tissue-specific" (light gray) HIF1a target categories. Bold dashed line represents the median with the thin dashed lines representing the upper and lower quartiles. p-values were calculated using the Kruskal Wallis One-Way ANOVA with Dunn's multiple comparisons test.
(L) qRT-PCR of canonical HIF1a genes *Pdk1* and *Bnip3* and non-canonical HIF1a target genes *Dgat2* and *Foxo6* in physiological hypoxia (1% O2) compared to normoxia at acute (4 hours), intermediate (24 hours), and chronic (48 hours) timepoints. Data are presented as mean ± SEM from 4 technical replicates (individual wells).
(M) Targeted metabolomics for pyruvate and lactate in both sgVhl and sgVhl.2 OPCs (both in green) compared to Cas9 control OPCs (in blue). Data are presented in relative units as mean ± SD from 6 biological replicates. p-values were calculated using one-way ANOVA with Dunnett's multiple comparisons test.
(N) Gene ontology (GO) analysis of genes targeted by HIF1a specifically in melanocytes (beige), embryonic heart (purple), and T cells (magenta). The chart includes curated pathways with their rank based on their respective p-values.

FIGURE S3

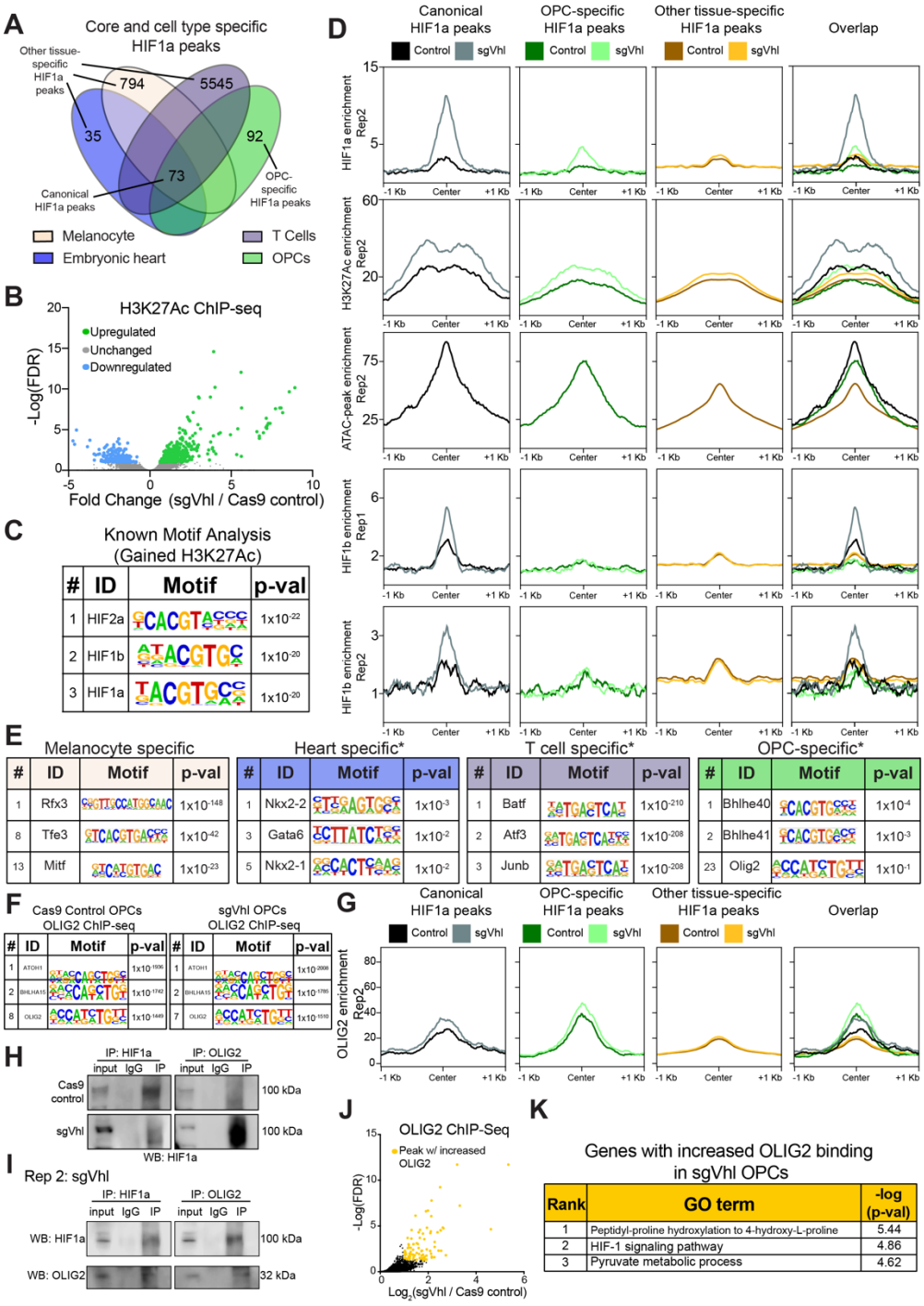

Figure S3. Chromatin Accessibility and Cell-Type-Specific Transcription Factors Define Non-Canonical HIF1a Targets, Related to Figure 3.

(A) Overlap of significant HIF1a peaks (FDR<0.001) across 4 different cell types giving canonical HIF1a peaks, OPC-specific HIF1a peaks, and “other tissue-specific” HIF1a peaks (combination of heart, T cell and melanocyte specific peaks). See also Table S2 for full list of cell-type-specific peaks for each cell type.

(B) Volcano plot of fold change in intensity of significant H3K27ac regions (FDR<0.001) between Cas9 control and sgVhl OPCs showing regions of significantly increased and decreased (FDR<0.1) H3K27ac in green and blue respectively.
(C) Table of known motifs in regions significantly enriched for H3K27ac in sgVhl OPCs compared to Cas9 control OPCs displaying the transcription factor name, motif, and p-value ranked in order of significance (# indicates rank out of all motifs from the analysis).
(D) Aggregate plots of HIF1a, H3K27ac, and HIF1b ChIP-seqs in Cas9 control and sgVhl OPCs as well as ATAC-seq in normal, non-transduced OPCs at canonical HIF1a peaks, OPC-specific HIF1a peaks, and "other tissue-specific" HIF1a peaks. Rep indicates replicate number.
(E) Table of known motifs significantly enriched in cell-type-specific HIF1a peaks in melanocytes (beige), heart (purple), T-cells (magenta) and OPCs (light green). Charts display the transcription factor name, motif, and p-value ranked in order of significance (# indicates rank out of all 440 motifs in the analysis and * indicates that HIF motifs were removed). See also Table S3 for full list of ranked motifs for each cell type.
(F) Table of known motifs significantly enriched under OLIG2 peaks (FDR<0.001) in Cas9 control and sgVhl OPCs. Charts display the transcription factor name, motif, and p-value ranked in order of significance. See also Table S4 for full list of ranked motifs.
(G) Aggregate plots of replicate OLIG2 ChIP-seq in Cas9 control and sgVhl OPCs at canonical HIF1a peaks, OPC-specific HIF1a peaks, and "other tissue-specific" HIF1a peaks.
(H) Western blot of HIF1a from total cell lysate (input), IgG control lysate, and lysate from pulldown (IP) of either HIF1a (on left) or OLIG2 (on right) in Cas9 control (top) and sgVhl OPCs (bottom).
(I) Western blot of HIF1a (top) and OLIG2 (bottom) from total cell lysate (input), IgG control lysate, and lysate from pulldown (IP) of either HIF1a (on left) or OLIG2 (on right) in sgVhl OPCs.
(J) OLIG2 peaks that display an increase in signal intensity in sgVhl OPCs compared to Cas9 control with statistically significant increased peaks highlighted in yellow (FDR<0.05). See also Table S4 for the list of significantly increased peaks.
(K) Gene ontology (GO) analysis of genes that exhibit a significant increase in OLIG2 binding (FDR<0.05, within 50 Kb) in sgVhl OPCs compared to Cas9 control OPCs. Table shows the rank of the GO term along with –log(p-value). See also Table S4 for the list of genes harboring significantly increased OLIG2 binding.

FIGURE S4

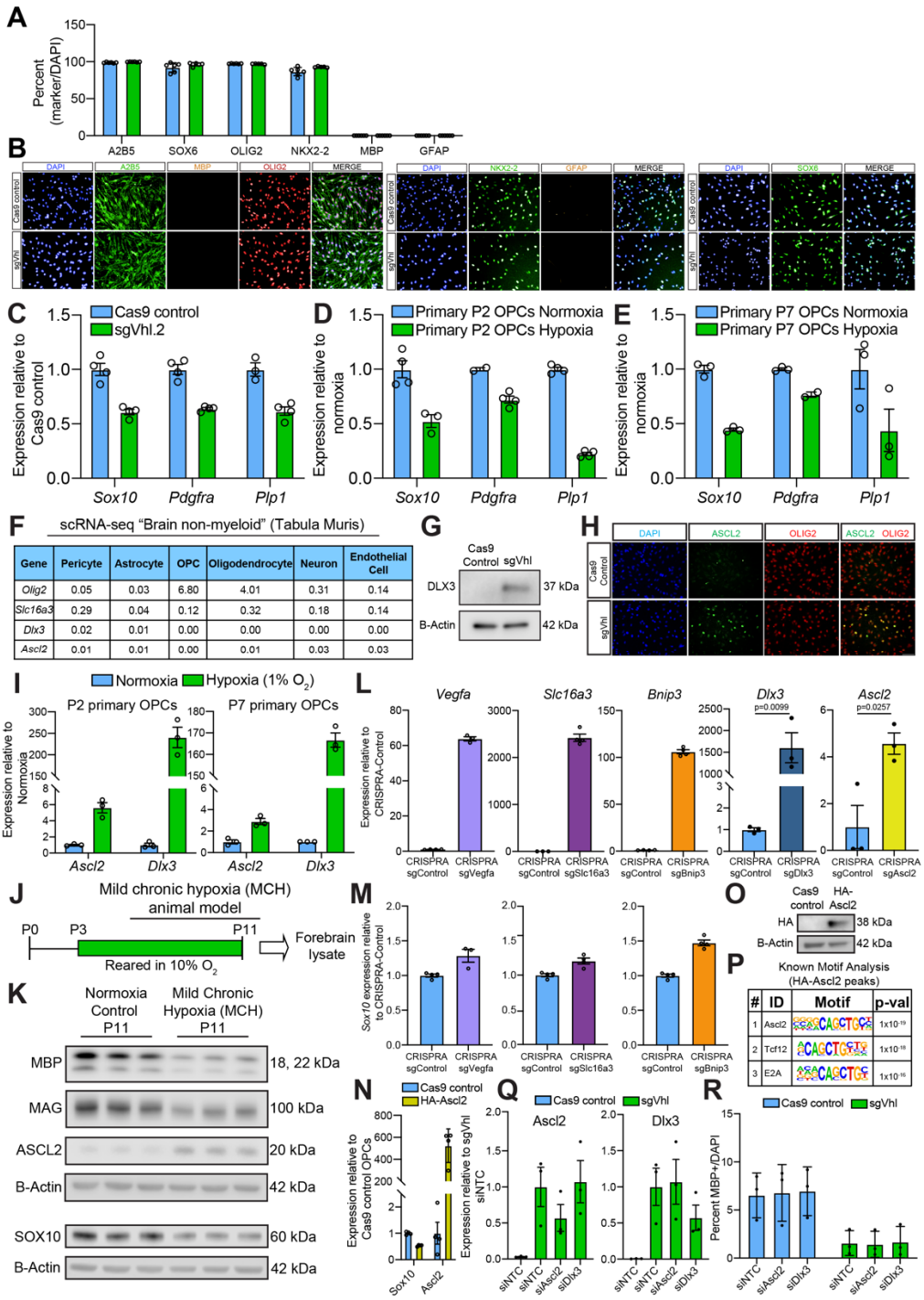

Gene	Pericyte	Astrocyte	OPC	Oligodendrocyte	Neuron	Endothelial Cell
Olig2	0.05	0.03	6.80	4.01	0.31	0.14
Slc16a3	0.29	0.04	0.12	0.32	0.18	0.14
Dlx3	0.02	0.01	0.00	0.00	0.00	0.00
Ascl2	0.01	0.01	0.00	0.01	0.03	0.03

Figure S4. OPC-specific HIF1a Targets *Ascl2* and *Dlx3* Suppress *Sox10* and Impair Oligodendrocyte Formation, Related to Figure 4.

(A) Quantification of lineage markers normalized to cell number (DAPI) between Cas9 control and sgVhl OPCs. Data represent mean ± SD from 6 technical replicates (individual wells) per condition.

(B) Immunocytochemistry of OPC markers A2B5, SOX6, OLIG2, and NKX2-2 along with the oligodendrocyte marker MBP and astrocyte marker GFAP in Cas9 control and sgVhl OPCs. Nuclei are marked by DAPI (in blue).

(C-E) qRT-PCR of *Sox10* and downstream SOX10 target genes *Pdgfra* and *Plp1* in sgVhl.2 (in green) compared to Cas9 control OPCs (in blue) (C), in primary postnatal day 2 (P2) *in vivo* derived mouse OPCs treated with physiological hypoxia (in green) compared to normoxia (in blue) (D), and in primary immunopanned postnatal day 7 (P7) *in vivo* derived mouse OPCs treated with physiological hypoxia (in green) compared to normoxia (in blue) (E). Data are presented as mean ± SEM from 3-4 technical replicates.
(F) Chart of publicly available single-cell RNA-seq data from non-myeloid cells of the brain for expression of *Dlx3*, *Ascl2* and *Slc16a3* with positive control *Olig2*, which marks OPCs and oligodendrocytes. Values are ln(1+CPM). CPM is counts per million reads.
(G) Western blot for DLX3 in sgVhl and Cas9 control OPCs.
(H) Immunocytochemistry (ICC) for ASCL2 (in green) and OLIG2 (in red) in Cas9 control and sgVhl OPCs. Nuclei are marked by DAPI (in blue).
(I) qRT-PCR of *Dlx3* and *Ascl2* in P2 and P7 primary *in vivo* derived OPCs treated with physiological hypoxia (1% O_2, in green) compared to normoxia (21% O_2, in blue). Data are presented as mean ± SEM from 3 technical replicates.
(J) Schematic highlighting the mild chronic hypoxia model of diffuse white matter injury in which mouse pups are reared in 10% oxygen from postnatal day 3 to 11 (P3 to P11) to model diffuse white matter injury of prematurity. Animals are sacrificed at postnatal day (P11) and their forebrains are isolated and lysed for protein.
(K) Western blots of forebrain lysates from P11 female C57Bl6 mice of myelin proteins MBP and MAG along with ASCL2 and SOX10 in animals reared in hypoxia from P3-P11 compared to normoxic reared mice. N= 3 female C57Bl6 mice per treatment group.
(L) qRT-PCR of *Vegfa*, *Slc16a3*, *Bnip3*, *Ascl2* and *Dlx3* in their respective CRISPRA OPCs compared to CRISPRA sgControl OPCs. Data are presented as mean ± SEM from 3-4 technical replicates for *Vegfa, Slc16a3,* and *Bnip3* and 3 biological replicates for *Ascl2* and *Dlx3*.
(M) qRT-PCR of *Sox10* in CRISPRA sgVegfa (light purple), sgSlc16a3 (magenta), and sgBnip3 (orange) OPCs compared to CRISPRA sgControl OPCs. Data are presented as mean ± SEM from 3-4 technical replicates.
(N) qRT-PCR of *Ascl2* and *Sox10* in Cas9 control and HA-Ascl2 OPCs. Data are presented as mean ± SEM from 4 technical replicates.
(O) Western blot of nuclear lysates for HA in Cas9 control and HA-Ascl2 OPCs.
(P) Table of known motifs significantly enriched under HA peaks (FDR<0.1) in HA-Ascl2 OPCs displaying the transcription factor name, motif, and p-value ranked in order of significance (# indicates rank out of all motifs from the analysis).
(Q) qRT-PCR of *Ascl2* and *Dlx3* in Cas9 control and sgVhl OPCs nucleofected with non-targeting control (NTC), Ascl2, or Dlx3 siRNAs. Data are presented as mean ± SEM from 3 biological replicates.
(R) Quantification of the percentage of mature (MBP+) oligodendrocytes formed from Cas9 control and sgVhl OPCs nucleofected with non-targeting control (NTC), Ascl2, or Dlx3 siRNAs. Data are presented as mean ± SD from 3 biological replicates.

FIGURE S5

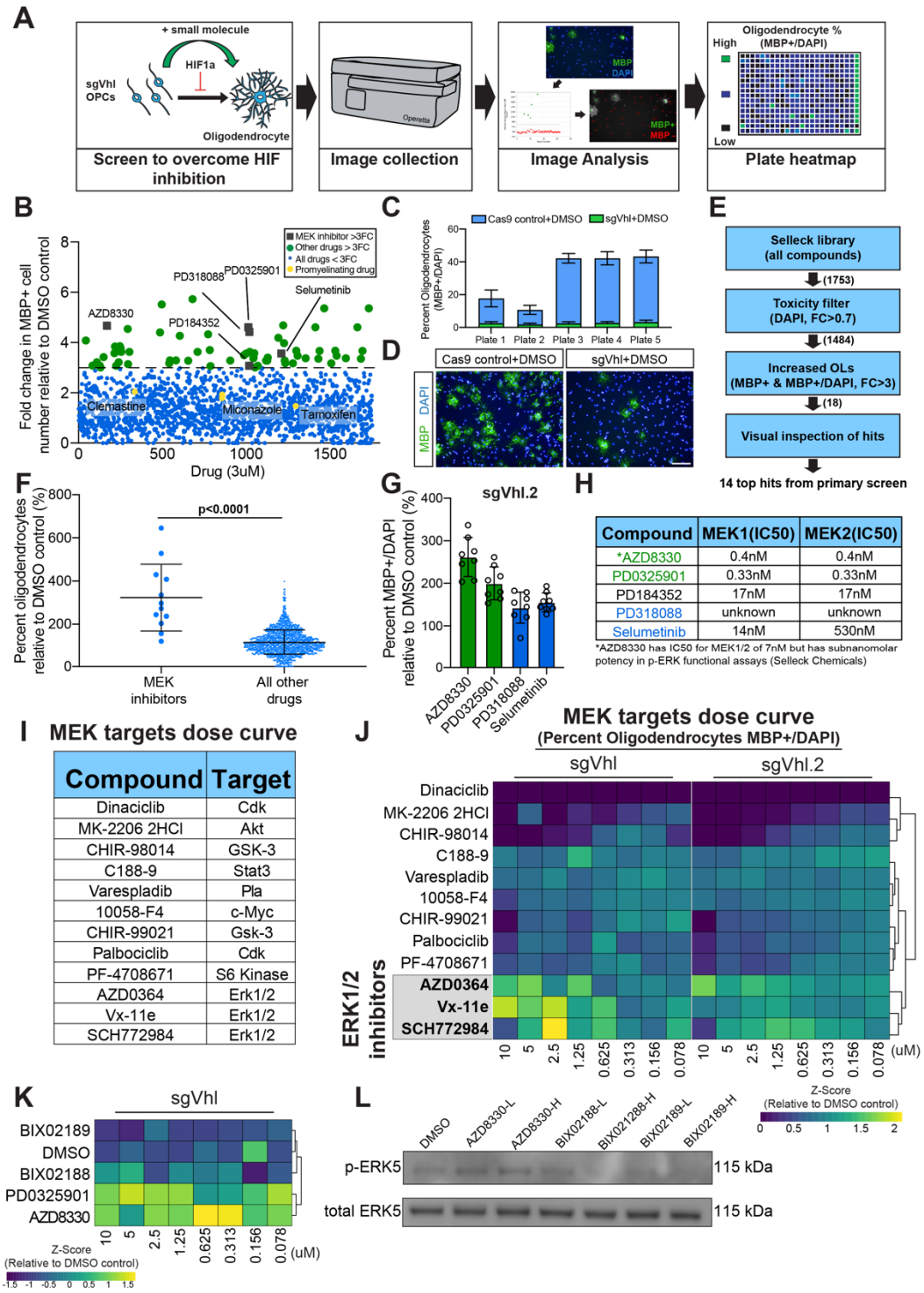

Figure S5. Inhibition of MEK/ERK Signaling Increases Oligodendrocyte Formation from sgVhl OPCs, Related to Figure 5.

(A) Schematic depicting the procedure for the primary bioactives screen to uncover compounds that increase oligodendrocyte formation from sgVhl OPCs.
(B) Primary bioactives library screen showing the effect of 1753 small molecules on number of oligodendrocytes (MBP+ cells) formed by sgVhl OPCs relative to DMSO treated sgVhl OPCs. The dotted line represents a 3-fold increase in oligodendrocyte

formation and compounds that clear this threshold are indicated as green dots. MEK inhibitors are highlighted as gray boxes and pro-myelinating drugs are highlighted as yellow dots. See also Table S5.
(C) Primary screen positive control (Cas9 control+DMSO) and negative control (sgVhl+DMSO) percent oligodendrocyte (MBP+/DAPI) metrics on a per plate basis. Data represent mean ± SD from 16 technical replicates (individual wells) per plate.
(D) Representative immunocytochemistry images of oligodendrocytes (MBP+ in green) from primary screen positive (Cas9 control+DMSO) and negative (sgVhl+DMSO) controls. Nuclei are marked by DAPI (in blue). Scale bars, 100μm.
(E) Schematic detailing the filtering steps starting with the bioactives library and narrowing down to top hits that are non-toxic (total DAPI FC<0.7), increased the number and percentage of oligodendrocytes (FC>3) and passed visual inspection to give the top 14 compound hits. Numbers in parentheses represent the number of drugs after each filtering step. See also Table S5.
(F) Quantification of the effect of all non-toxic MEK inhibitors (n=12) and other non-toxic drugs from the primary screen (n=1472) on the percentage of oligodendrocytes from sgVhl OPCs relative to DMSO treated sgVhl OPCs. Data are presented as mean ± SD. p-values were calculated using the Mann-Whitney test.
(G) Collapsing all tested doses into one overall average shows the ability of each MEK inhibitor to increase the formation of oligodendrocytes (MBP+/DAPI) from sgVhl.2 OPCs relative to DMSO treatment. Green and blue columns represent the most and least effective compounds respectively. Data are presented as the mean ± SD of all 8 doses from a single dose curve plate.
(H) Table of IC50 values for MEK1 and MEK2 for the top MEK inhibitors AZD8330, PD035901, PD184352, and Selumetinib. IC50 is still currently unknown for PD318088.
(I) Table of drugs targeting other MEK targets including the drug name and canonical target of the drug.
(J) Heatmap representation of the 8-point dose curve performed for all 12 drugs in the MEK target dose curve plate shown as row Z-score. Data in the heatmap is the fold change in percent oligodendrocytes (MBP+/total DAPI) in sgVhl and sgVhl.2 OPCs relative to their respective DMSO negative controls. Rows were sorted by unsupervised hierarchical clustering and columns are in order from high (10μM) to low dose (78nM) of drug. ERK1/2 inhibitors are highlighted in gray and bold. Data are presented as the mean for each drug at each dose from 2 separate dose curve plates for both sgVhl and sgVhl.2 OPCs.
(K) Heatmap representation of the 8-point dose curve performed for DMSO, AZD8330, and MEK5 inhibitors (BIX02189 and BIX02188) shown as row Z-score. Data in the heatmap is the fold change in percent oligodendrocytes (MBP+/total DAPI) in sgVhl OPCs relative to the DMSO negative control. Rows were sorted by unsupervised hierarchical clustering and columns are in order from high (10μM) to low dose (78nM) of drug. Data are presented as the mean for each drug at each dose from 3 separate dose curve plates.
(L) Western blot of p-ERK5 and total ERK5 from sgVhl OPCs treated with high (3 μM) and low (300nM) doses of AZD8330, BIX02188, and BIX02189. Data represent results from a single biological replicate.

FIGURE S6

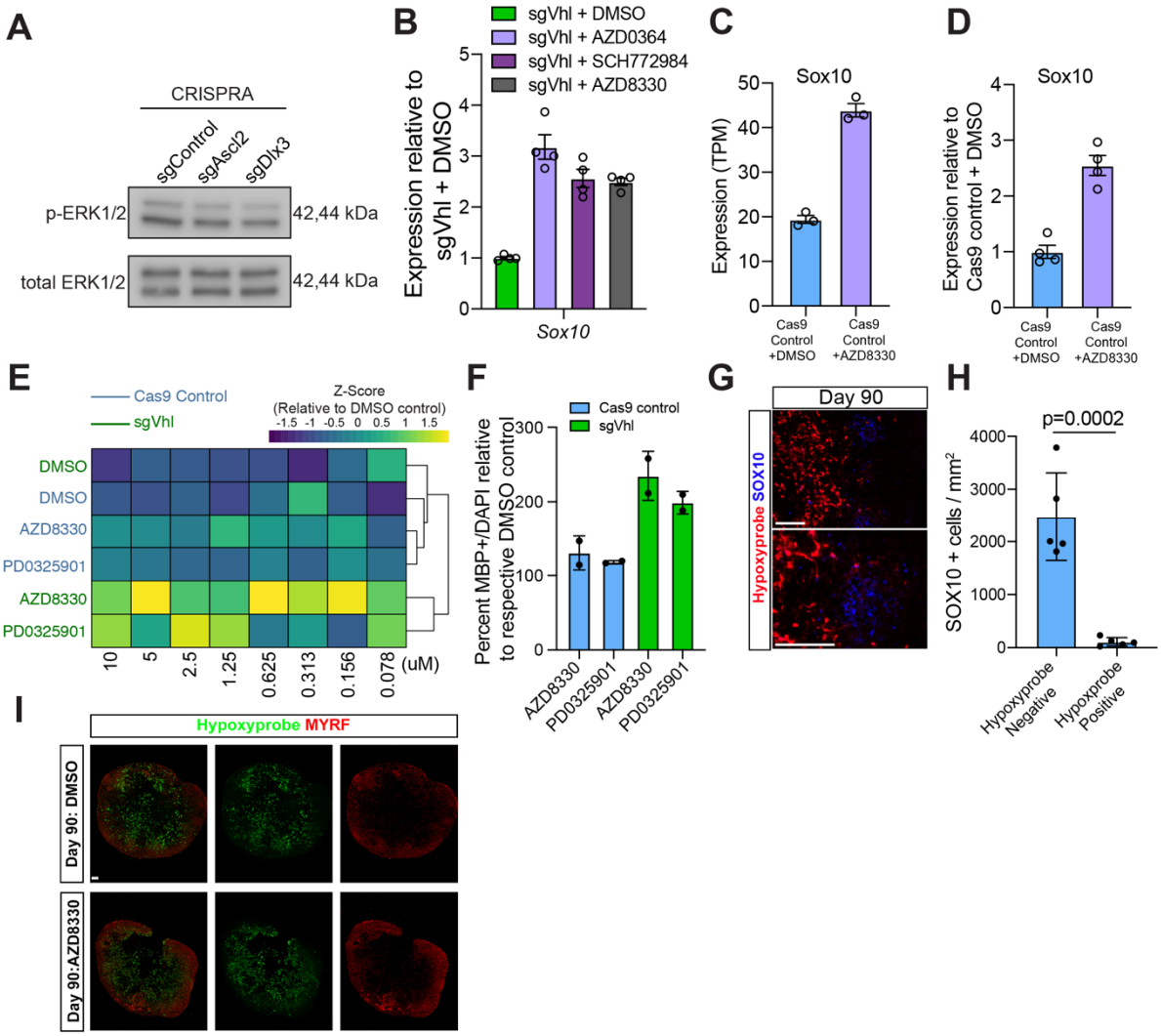

Figure S6. Inhibition of MEK/ERK Signaling Drives *Sox10* Expression in sgVhl OPCs, Related to Figure 6.

(A) Western blot of phosphorylated ERK1/2 (p-ERK1/2) and total ERK1/2 of sgControl, sgAscl2, and sgDlx3 CRISPRA OPCs. Data represent results from a single biological replicate.
(B) qRT-PCR of *Sox10* in sgVhl OPCs treated with DMSO, AZD0364 (1μM, in purple), SCH772984 (1μM, in magenta) or AZD8330 (300nM, in gray) for 14hrs. Data are presented as mean ± SEM from 4 technical replicates.
(C) Quantification of the normalized number of transcripts (TPM) for *Sox10* in Cas9 control+DMSO (in blue), and Cas9 Control+AZD8330 OPCs (in purple). OPCs were treated with either DMSO or 300nM AZD8330 for 14 hours. Data represent mean ± SD from 3 independent RNA-seq replicates.
(D) qRT-PCR of *Sox10* in Cas9 control OPCs treated with DMSO (in blue) or AZD8330 (300nM, in purple) for 14 hours. Data are presented as mean ± SEM from 4 technical replicates.

(E) Heatmap representation of the 8-point dose curve performed for DMSO, AZD8330, and PD0325901 in Cas9 control (in blue) and sgVhl (in green) OPCs shown as row Z-score. Data in the heatmap is the fold change in percent oligodendrocytes (MBP+/total DAPI) relative to the respective DMSO negative control. Rows were sorted by unsupervised hierarchical clustering and columns are in order from high (10μM) to low dose (78nM) of drug. Data are presented as the mean for each drug at each dose from 2 separate dose curve plates.
(F) Collapsing all tested doses into one overall average shows the ability of each MEK inhibitor to increase the formation of oligodendrocytes (MBP+/DAPI) from Cas9 control (in blue) and sgVhl OPCs (in green) relative to DMSO. Data are presented as the mean ± SD of the averages of all 8 doses for each drug from 2 separate dose curve plates.
(G) Representative immunohistochemistry images at low and high magnification of the edge of a DIV 90 oligocortical spheroid for SOX10+ cells (in blue) and hypoxic regions (hypoxyprobe in red). Scale bars, 100μM.
(H) Quantification of SOX10+ cells (SOX10+ / mm^2) in the normoxic region of the spheroid (hypoxyprobe negative) and hypoxic region of the spheroid (hypoxyprobe positive) in DIV 90 spheroids. Data represent mean ± SD from 5 individual spheroids. p-values were calculated using Student's two-tailed t-test.
(I) Representative immunohistochemistry images of entire DIV 90 oligocortical spheroids that had been treated from DIV 70-74 with either DMSO or 300nM AZD8330 for oligodendrocytes (MYRF+ in red) and hypoxic regions (hypoxyprobe in green). Scale bar, 100μM.